Catalysis Today 157 (2010) 263–269

Contents lists available at ScienceDirect

Catalysis Today

journal homepage: www.elsevier.com/locate/cattod

Screening of ceria-based catalysts for internal methane reforming in low temperature SOFC

Cyril Gaudillère[a,b,*], Philippe Vernoux[a], Claude Mirodatos[a], Gilles Caboche[b], David Farrusseng[a]

[a] Université Lyon 1, CNRS, UMR 5256, IRCELyon, Institut de recherches sur la catalyse et l'environnement de Lyon, 2 avenue Albert Einstein, F-69626 Villeurbanne, France
[b] Institut Carnot de Bourgogne, UMR 5209 CNRS, Université de Bourgogne, 9 avenue Alain Savary, BP 47870, F-21078 Dijon, France

ARTICLE INFO

Article history:
Available online 29 March 2010

Keywords:
Methane oxidation and reforming
Heterogeneous catalysis
SOFC anode
Cerium oxide
Combinatorial screening

ABSTRACT

Ceria-based catalysts have been assessed for internal methane reforming at low temperature (400–600 °C) in Solid Oxide Fuel Cell (SOFC). A combinatorial library of 15 metal (Cu, Pt, Ni) supported ceria was prepared using wet impregnation method. The ceria-based oxides are undoped or doped with metal transition (Zr) or by rare earth (Gd or Pr). The effect of the metal, the dopant and the surface area on the catalytic performances was investigated in high-throughput manner using a 16-parallel reactor. The catalysts were assessed in two different conditions, (i) in CH_4 rich condition and (ii) in model reformate condition. Catalytic performances are very metal depending. In dry conditions, Cu-based catalysts do not produce H_2 whereas Ni-catalysts are very active despite low carbon balance. However, when water and CO_2 are added in the feed, the nature of the ceria plays an important role in the catalytic performances. At low temperature ($T < 550$ °C), most of Ni/ceria catalysts are not active under reformate conditions at low temperature while Pt catalysts appear more robust with respect to the conditions. From unsteady state parallel studies, we suggest that surface hydroxyl on ceria are the active species.

1. Introduction

Solid Oxide Fuel Cells (SOFCs) are considered as a very efficient technologies to produce electrical energy from H_2. However, H_2 storage and distribution issues make its use non-appropriate for transport, domestic and remote applications. On the other hand, the internal reforming is an attractive solution to overcome H_2 storage and distribution issues. The large resource, high H/C ratio and distribution infrastructure make natural gas the fuel of choice [1]. Unfortunately, direct hydrocarbon reforming in conventional SOFC causes long term issues due to coke formation over Ni/ZrO_2 based anodes [2]. Due to material limitations, conventional SOFC systems operate at very high temperatures (1000 °C). Intense R&D efforts aim at decreasing the operating temperature in order to limit ageing issues of the diverse components including interfaces and sealing. However, to the best of our knowledge, the development of catalysts for internal reforming of methane is scarce for low temperature (400–600 °C). In a previous high-throughput screening [3], we have identified ceria-based catalysts as potential candidates for H_2 production at low temperature. We found out that the performances in autothermal conditions were very influenced by the nature of the metal and ceria dopant.

The objective of this study is to assess ceria-based catalysts for the H_2 production from methane at low temperature in a SOFC. Among the questions that we have addressed: Can Ni, the usual reforming metal at high temperature, be active at low temperature? Can Cu be an alternative metal with reduced coking effects? What are the effects of H_2O and/or CO_2 on the catalytic performances and time on stream stability?

Among the various scenarios using natural gas as fuel [4], two technological options can be considered: (A) the anode is fed by methane stream. CO and H_2 can be obtained from selective oxidation while H_2O and CO_2 are produced in situ and then can be further used as reforming agents (steam and dry reforming). In this scenario, the main objective is to investigate methane activation on suitable catalysts enclosed into the anode layer in SOFC operating conditions, i.e. by simulating a continuous low flow of oxygen coming from the electrolyte. (B) The anode is fed directly by a process gas which is basically a methane rich mixture with variable amounts of H_2O and CO_2 corresponding to a downstream reformate feed (CO_2, H_2, CO, H_2O and CH_4) in domestic application [5] or a biogas composition obtained from biomass or municipal waste fermentation.

In this study, we report the synthesis and parallel testing of a wide range of modified metal impregnated ceria-based catalysts as potential SOFC anodes at low temperature through two potential scenarios (A and B).

* Corresponding author at: Université Lyon 1, CNRS, UMR 5256, IRCELyon, Institut de recherches sur la catalyse et l'environnement de Lyon, 2 avenue Albert Einstein, F-69626 Villeurbanne, France.
E-mail address: cyril.gaudillere@ircelyon.univ-lyon1.fr (C. Gaudillère).

0920-5861/$ – see front matter © 2010 Elsevier B.V. All rights reserved.
doi:10.1016/j.cattod.2010.02.062

2. Experimental

2.1. Samples preparation

Five cerium-based powders were supplied by Rhodia (Ce-H, CeZr-H, CePr-H and CeGd-L) and purchased from Nextech Materials (CeGd-H). Compositions and surface area data are given in Table 1. For the same CGO composition, two samples with high (H) and low (L) surface area have been tested. The 15 supported catalysts were prepared by wetness impregnation by combining the 5 different supports and 3 metals (Pt, Ni, Cu) (Table 1). Typically, the wet impregnation was carried by the dissolution of appropriated metal salt in water at concentrations approaching saturation. The support was impregnated and water was added until all the powder is soaked. The slurry was vigorously stirred for 2 h, dried in oven at 100 °C for 1 h then calcined under static air at 500 °C for 8 h with a rate of 60 °C/h.

2.2. Samples characterization

Prior catalytic tests, all catalysts were characterized by X-ray diffraction (XRD) using a Bruker D5005 Diffractometer with the Cu Kα radiation. The amount of metal (Ni, Cu, Pt) was measured by ICP (Activa Horiba). Porous structural data are summarized in Table 1. Transmission electron microscopy (JEOL 2010 LaB6) studies were carried out on fresh Ce-H sample and Pt-Ce-H samples (after Pt impregnation and calcination). The specific surface areas (BET method) were determined by N_2 physisorption at 77 K (ASAP 2020 Micromeritics; desorption conditions 10^{-2} mbar; 300 °C for 3 h) for all samples at different stages; cerium-based supports as received and fresh catalysts (after impregnation and calcinations).

2.3. Testing equipments and methods

Catalytic tests were carried out on the Switch 16 parallel reactor (AMTEC GmbH-CNRS) as described in [6]. This multi-channel device consists of 16 parallel reactors in Inconel™ with two independent feeding systems. In this study, the switching 16 port valve allows (i) to regenerate catalysts under air after gas chromatography (GC) sampling is achieved; (ii) to perform unsteady state testing by switching the feed from air to methane and recording on-line. Exhaust gases were analysed on-line by gas chromatography (GC HP 6950 and 6980). Water introduced or produced during the reaction was condensed in a Peltier cooler placed before the GCs. For unsteady state experiments, the analyses were performed with an on-line mass spectrometer (Inficon IPC-400). Prior catalytic runs, catalysts were stabilized at 600 °C for 4 h under test conditions and then cool down to 400 °C. When the targeted reaction temperature is reached, the downstream stream is analysed in an empty reactor in order to measure blank activity. Then, one reactor is fed by the inlet stream (see below) while the 15 reactors are regenerated under air (50 mL/min) conditions. In order to ensure that the catalytic performances are measured under steady state conditions, duplicate samplings at different time were carried out, i.e. after 12 and 22 min of time on stream. In all cases, the analyses differ less than 1% showing that the catalysts are equilibrated. The reported values correspond to the average of these two analyses. Then, a subsequent reactor is selected for a catalytic run. After all runs are completed at a given temperature, the temperature is heated up to the next plateau, from 400 to 600 °C every 25 °C at atmospheric pressure. The 15 reactors are filled with 100 mg of catalysts and the last reactor is free of catalysts and used as a blank test. Scenario A is simulated with a methane-to-oxygen ratio of 15:2 (7.5:1 mL/min), argon as balance (41.5 mL/min) and a total flow of 50 mL/min. Scenario B was studied as previously with a feed consisting in 20% of steam (10 mL/min) and then 20% of steam (10 mL/min) and 5% of carbon dioxide (2.5 mL/min) added to the former CH_4-O_2 mixture. Unsteady state experiments over Pt-CePr-H and Ni-CePr-H were performed to investigate reaction mechanism. Diluted methane was fed on fully oxidized catalysts and a flow of 5% of methane diluted in argon was fed for 4 min.

For all cases, the methane conversion and H_2 yield are calculated as:

$$X_{CH_4} = \left(1 - \frac{CH_{4_{outlet}}}{CH_{4_{inlet}}}\right) \times 100 \quad \text{and}$$

$$Y_{H_2} = \frac{H_{2_{outlet}}}{2CH_{4_{inlet}} + H_2O_{inlet}} \times 100$$

The carbon balance was defined as the fraction of all the carbon atoms recovered at the reactor outlet over all the carbon atoms fed into the reactor: $Z = \frac{\sum_{Compounds} C_{outlet}}{\sum_{Compounds} C_{inlet}}$.

A value below 1 means a carbon loss (carbonaceous species deposition).

CO selectivities were calculated by:

$$S_{CO} = \frac{CO_{outlet}}{CO_{inlet} + CO_{2_{outlet}}} \times 100$$

The thermodynamic equilibrium data were calculated on the basis of the inlet gas composition and including all the potential products formation under various atmosphere conditions. The Gibbs free energy was minimized by using the software Outokumpu HSC (ver. 4.1). These calculations were conducted for temperatures between 400 and 600 °C and at a total pressure of 1 bar. The relevant species are CH_4, O_2, H_2, CO, CO_2 and H_2O for the gas phase and graphitic carbon for the solid phase. The considered reactions which can take place under the present operating conditions are (ΔH values are given for T = 298 K):

Methane total and selective oxidations:

$$CH_4 + 2O_2 = CO_2 + 2H_2O \quad \Delta H = -798\ \text{kJ/mol} \tag{1}$$

and

$$CH_4 + (1/2)O_2 = CO + 2H_2 \quad \Delta H = -58\ \text{kJ/mol} \tag{2}$$

Methane steam and dry reforming:

$$CH_4 + H_2O = CO + 3H_2 \quad \Delta H = 206\ \text{kJ/mol} \tag{3}$$

and

$$CH_4 + CO_2 = 2CO + 2H_2 \quad \Delta H = 261\ \text{kJ/mol} \tag{4}$$

Water gas shift reaction:

$$CO + H_2O = CO_2 + H_2 \quad \Delta H = -41\ \text{kJ/mol} \tag{5}$$

Two sets of reactions have to be considered for carbon formation and/or consumption:

$$\text{Methane cracking}: CH_4 = C + 2H_2 \quad \Delta H = 75\ \text{kJ/mol} \tag{6}$$

Carbon steam and dry reforming (Boudouard reactions):

$$CO + H_2 = C + H_2O \quad \Delta H = -133\ \text{kJ/mol} \tag{7}$$

and

$$2CO = C + CO_2 \quad \Delta H = -172\ \text{kJ/mol} \tag{8}$$

3. Results

3.1. Catalysts characterization

Whatever the ceria substitution, the fluorite structure is maintained for all samples as evidenced by X-ray diffraction. The absence

Table 1
Catalysts composition and textural features.

Ceria doping	Specific surface area (m^2/g)	Me	Loading (wt%)	Specfic surface area after calcination (m^2/g)	Notation
Undoped		Pt	3.88	133	Pt-Ce-H
Undoped	237	Ni	3.18	201	Ni-Ce-H
Undoped		Cu	2.69	193	Cu-Ce-H
30% ZrO_2		Pt	2.04	90	Pt-CeZr-H
30% ZrO_2	127	Ni	2.16	103	Ni-CeZr-H
30% ZrO_2		Cu	4.05	110	Cu-CeZr-H
10%Pr_6O_{11}		Pt	3.95	163	Pt-CePr-H
10%Pr_6O_{11}	174	Ni	3.48	167	Ni-CePr-H
10%Pr_6O_{11}		Cu	3.85	160	Cu-CePr-H
10% Gd_2O_3		Pt	2.65	<15	Pt-CeGd-L
10% Gd_2O_3	15	Ni	3.87	<15	Ni-CeGd-L
10% Gd_2O_3		Cu	2.56	<15	Cu-CeGd-L
10% Gd_2O_3		Pt	4.24	151	Pt-CeGd-H
10% Gd_2O_3	213	Ni	5.02	129	Ni-CeGd-H
10% Gd_2O_3		Cu	4.42	143	Cu-CeGd-H

of reflexes corresponding to the metal phase can be interpreted as a high metal dispersion [7]. It is confirmed by the TEM image of Pt-Ce-H (Fig. 1a) showing a high degree of crystallisation with lattice fringes and the uniform size of impregnated platinum of about 2 nm (Fig. 1b), corresponding to an estimated dispersion of about 60%. As seen in Table 1, ICP analyses reveal a metal loading of $3.5\% \pm 0.9$. The scattering of these contents might come from early precipitation upon the impregnation. As a general trend, whatever be the dopant or the absence of dopant, the larger the fresh material BET area, the larger the sintering effect after calcination at 500 °C. Thus, the decrease is more pronounced for CeGd-H (35%) whereas it is limited for CePr-H (9%). No further sintering was observed over CeGd-L samples whatever the impregnated metal. The BET area of others catalysts remains higher than 100 m^2/g, thus offering the potentiality for high metal dispersion.

3.2. Catalysts screening for methane reforming (Scenario A)

3.2.1. Reforming in rich methane stream in absence of H_2O and CO_2

Methane conversion. Methane conversion as a function of the temperature is shown in Fig. 2. No significant deactivation was noticed after 22 min on stream. Obviously, catalytic results are strongly metal dependant. (i) All Cu impregnated catalysts (not shown) are poorly active with conversion of about 6 (±1)% conversion. Whatever the dopant and the temperature, Cu/ceria samples behave as methane combustion catalysts. The calculated CH_4 conversion which would only arise from total oxidation with full oxygen conversion is 6.6%. (ii) For Pt and Ni-based catalysts, from 450 °C, all the oxygen is consumed while methane conversion still increases with temperature in the range 450–600 °C meaning that other reactions than methane oxidation take place. As shown in Fig. 2, the conversions are quite far from thermodynamics. Over Pt-based catalysts, it represents only about 20% and 30% of the thermodynamic equilibrium at 400 and 600 °C respectively. For Ni-based oxides, methane conversion is closer to thermodynamic values and raises with temperature significantly between 500 and 600 °C. Besides, any significant discrepancy with the dopants and the high/low surface areas (deviation of ±2.5%) is noticed for Pt catalysts. On the other hand, different conversions for Ni-based catalysts have been measured. Highest conversions are found for Ni-CeGd-L and Ni-CePr-H. Surprisingly, any significant trends related to the evolution of the surface area or the dopant can be observed.

CO selectivity and hydrogen yield. High CO selectivities were obtained for both Pt and Ni catalysts, especially at high temperature. Selectivities followed more or less closely the thermodynamic trends, indicating that the WGS equilibrium (5) was roughly achieved. CO selectivity increases with temperature spanning over a wide range, increasing from about 0 at 450 °C to 95% at 600 °C. This observation is consistent with the promotion of the WGS equilibrium confirmed by the decrease of CO_2 content increasing the temperature. Based on methane conversion, hydrogen yields follow a similar trend as observed in Fig. 2. Ni-based systems are found to give hydrogen yields about two times higher than Pt-based systems. Thus, at 600 °C for the CePr-H support, the H_2 yield is about 16% over Pt and 30% over Ni. Cu-based catalysts exhibit no or any syngas production over the whole explored temperatures and are

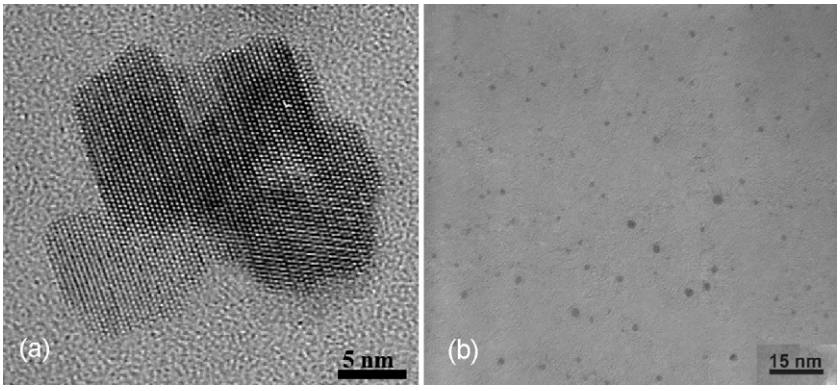

Fig. 1. TEM micrographs of the CeO_2 support (a) and of the Pt-Ce-H sample (b).

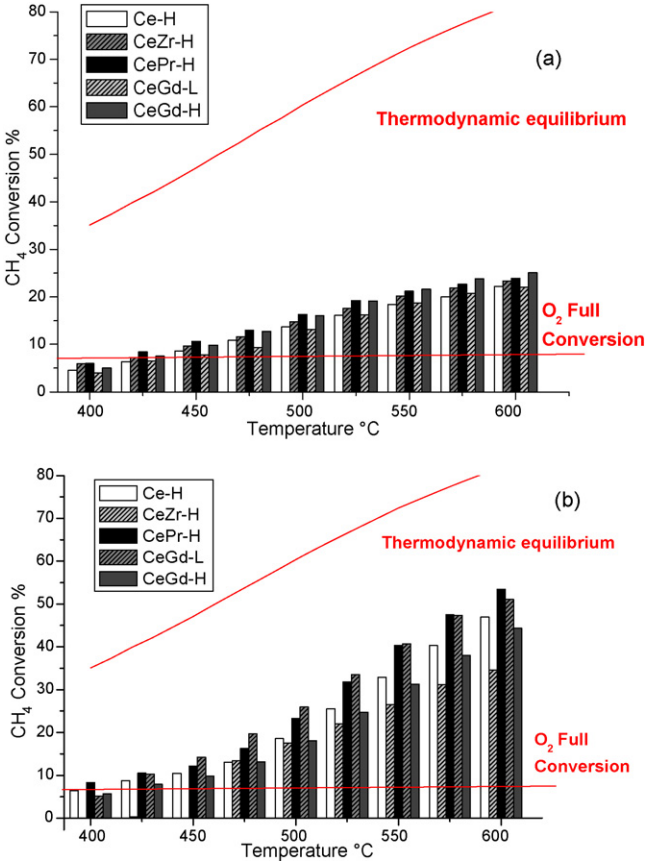

Fig. 2. CH_4 conversion as a function of temperature over Pt (a), Ni (b) and Cu (c) impregnated support tested under the reacting flow: CH_4:O_2 = 15:2 with Ar as balance, flow rate: 50 mL/min.

not appropriate catalysts for our concern. Thus, they will not be discussed further in the following.

Carbon balance. Pt and Ni impregnated catalysts show a deficient carbon balance which slightly decreases at 450 °C for all samples and significantly drops from 550 and 600 °C on Ni and Pt-based systems, respectively. Under these specific conditions, the reaction of methane cracking (6) takes place and carbonaceous species are trapped on the surface. This is in line with the fact that the higher the methane conversion, the lower the carbon balances. For instance, carbon balance value is 0.57 for Ni-CePr-H at 57% of conversion against 0.87 for Pt-CePr-H at 23.9% of conversion at 600 °C. This trend can be explained by the fact that due to the low amount of oxygen in the feed, most of the methane conversion is insured by methane cracking at high conversion. Fig. 3 presents the carbon balance as a function of CH_4 conversion per percent of metal loading in order to compare more quantitatively the methane cracking ability. As can be seen, a clear difference between Pt and Ni-based catalysts sensitivity to support doping and surface area is revealed: (i) For the Pt-based systems (filled square), no significant difference on carbon balance trends between different supports is observed. It suggests that under this condition, the rate determining step of the methane conversion is controlled by the activation step on metal, and not by a step involving the support. (ii) For the Ni-based catalysts (empty square), one can note a marked influence of support nature for a given conversion: at 7%, carbon balance values range from 0.95 for Ni-CeZr-H to 0.73 for Ni-CePr-H pointing out a strong involvement of the support in the cracking process. Similarly, for a given dopant (e.g. Gd), the surface area also plays a role, the cracking (related to the carbon storage) being more efficient on a low surface area support.

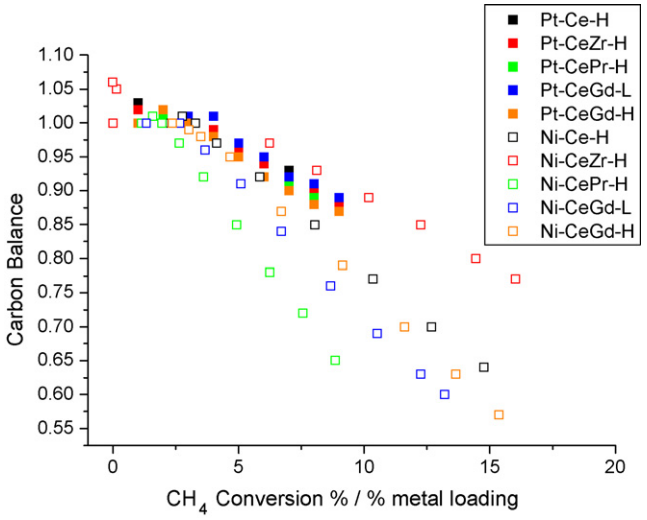

Fig. 3. Carbon balance as a function of the ratio (CH_4 conversion %:% metal loading) and temperature over Pt and Ni-based catalysts under the reacting flow: CH_4:O_2 = 15:2 with Ar as balance, flow rate: 50 mL/min.

3.2.2. *Reforming presence of H_2O and CO_2 (Scenario B)*

3.2.2.1. Effect of water. Methane conversion. As expected from steam addition, a marked increase in methane conversion and H_2 production can be noticed. Over Pt-based catalysts (not shown), methane conversion is typically doubled with respect to dry conditions and the gap with thermodynamic decreased. Such improvement with water addition has been reported [8]. For example, Pt-CePr-H shows a conversion of 53% at 600 °C against 24% without steam. In contrast to Scenario A, net discrepancies between supports are noticed where a Pr doping allows to double the conversion at 600 °C with respect to pure ceria support, Pt-CePr-H (53%) and Pt-Ce-H (24%). For some Pt and Ni-based systems, the methane conversion does not exhibit a gradual increase with temperature. For instance, the catalysts Ni-Ce-H presents (Fig. 4) a sharply increase at around 475 °C, then a slight drop until 550 °C and then a regular increase until 600 °C. These odd conversion changes might indicate changes in the catalyst redox properties and therefore reaction mechanism. For Ni-based catalysts and for most supports (but at various extents), a kind of "light-off" effect is observed in the temperature range 400–525 °C (Fig. 4). Water strongly inhibit methane conversion until 425 °C on Ni-CeGd-H, 450 °C on Ni-Ce-H, Ni-CePr-H, Ni-CeGd-L and 525 °C on Ni-CeZr-H.

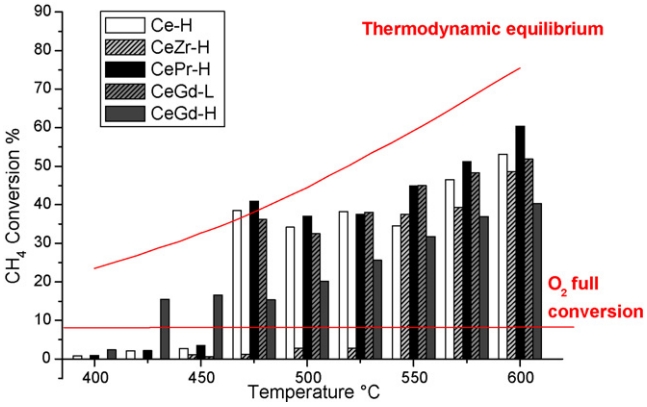

Fig. 4. CH_4 conversion as a function of temperature over Ni impregnated support under the reacting flow: CH_4:O_2:H_2O = 15:2:20 with Ar as balance, flow rate: 50 mL/min.

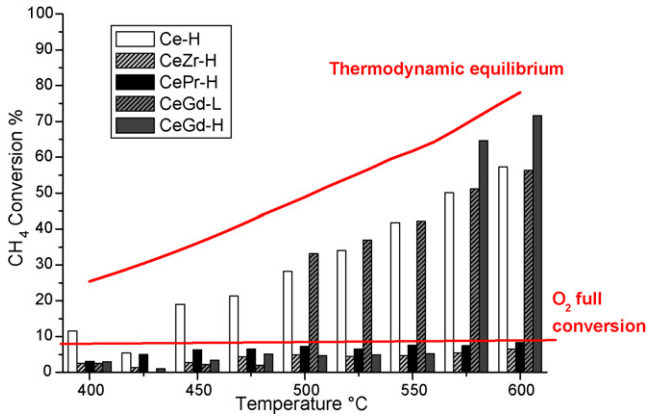

Fig. 5. CH_4 conversion as a function of temperature over Ni impregnated support under the reacting flow: CH_4:O_2:H_2O:CO_2 = 15:2:20:5 with Ar as balance, flow rate: 50 mL/min.

CO selectivity and hydrogen yield (data not shown). On Pt-based catalysts, the CO production is negligible below 500 °C, most probably due to CO oxidation which is strongly promoted by Pt. From 500 °C, the CO selectivity increases with the temperature to values higher than 60% at 600 °C with Pt-CeZr-H (Sco = 40%) being the only exception. For Ni-based catalysts, the CO selectivity increases with temperature up to 78% (case of Ni-CeGd-H at 600 °C). In contrast to dry conditions, hydrogen yield tends to follow closely the thermodynamic equilibrium in presence of steam water. For instance Pt-CePr-H, the H_2 yield is 43% in water conditions against 17% in dry conditions at 600 °C. The impact of the support nature is much more pronounced whatever the impregnated metal with for example 48% over CeZr-H and 13% over Ce-H over Pt-based catalysts at 600 °C.

Carbon balance (data not shown). In contrast to dry conditions, strong discrepancies in the carbon balance can be observed with respect to the nature of the support for Pt-based catalysts. For Ni-based catalysts, water limits the carbon deposition like previously described by Roh et al. [9] but higher temperature. Carbon balance values are always much higher than under Scenario A.

3.2.2.2. Effect of the mixture water and carbon dioxide. Methane conversion. For Pt-based catalysts, we can note an improvement of methane conversion when CO_2 is added to the wet stream. For example, CePr-H exhibits 69% of methane conversion against 52% without carbon dioxide feeding. We can observe significant difference with respect to the supports. CePr-H is here again the most active support followed by CeGd-H, CeZr-H, CeGd-L and then Ce-H. CO_2 addition enables to close the gap between experimental values and thermodynamic simulation. Pt-CePr-H exhibits CH_4 conversions of 17% and 69% (25.4% and 78.1% by thermodynamic simulation) at 400 and 600 °C, respectively. For Ni-based catalysts, three different trends can be observed as shown in Fig. 5. For, Ni-Ce-H, we can see an increasing methane conversion on the whole temperature range. In contrast, the conversion is very limited for Ni-CeGd-L and -H catalysts until a kind of "light-off" is observed (500 and 575 °C, respectively). Such temperature and support dependant inhibition was already pointed out in presence of water, for lower temperature range however (425 and 475 °C, respectively). Finally, the presence of CO_2 inhibits entirely the reforming for Ni-CePr-H and Ni-CeZr-H in the considered temperature range.

CO selectivity and hydrogen yield. Values of CO selectivity are very poor for Pt-based catalysts until 500 °C. The increase of hydrogen and carbon monoxide productions is associated to the promotion of dry methane reforming (reaction (4)). Very scattered results can be

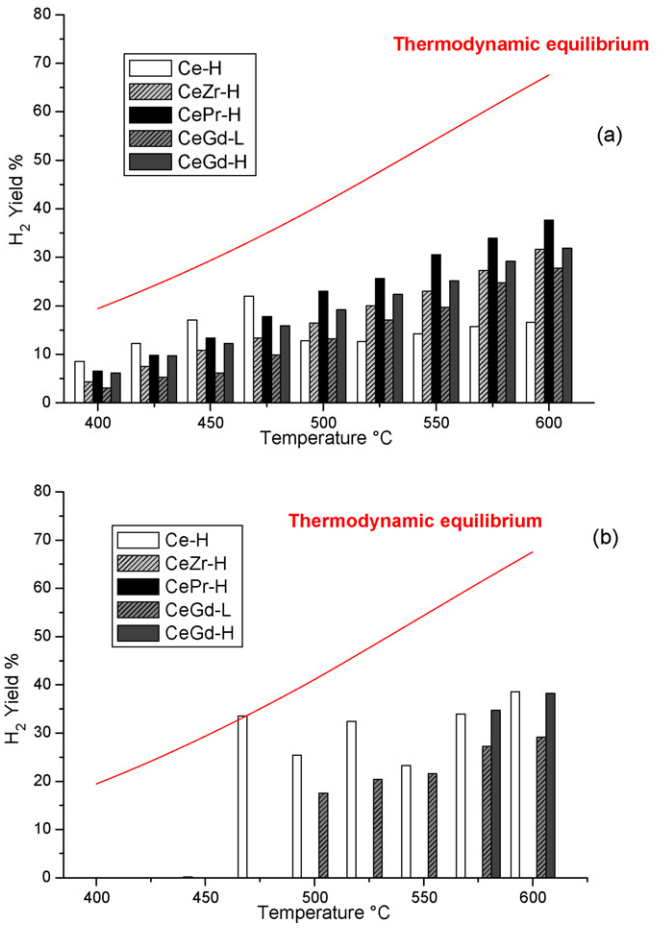

Fig. 6. H_2 yield as a function of temperature over Pt (a), Ni (b) impregnated support under the reacting flow: CH_4:O_2:H_2O:CO_2 = 15:2:20:5 with Ar as balance, flow rate: 50 mL/min.

observed for Ni-based catalysts. The hydrogen yield does not follow an activated profile with temperature for Ni-Ce-H. A slight decrease is noticed at high temperature compared with tests performed with addition of water [10]. This global decrease of hydrogen production associated with increasing CO selectivities is characteristic of the Reverse Water Gas Shift reaction (5) (Fig. 6).

Carbon balance. The simultaneous addition of water and CO_2 give a very different picture. Active Ni-based catalysts exhibit low carbon balance whatever the formulation. In contrast, the nature of the dopants has marked effect for Pt-based catalysts. The undoped Pt-Ce-H accumulates carbonaceous species the most whereas Gd and Zr doped ceria are less prone to carbon accumulation although they are the most active catalysts (Fig. 7).

3.3. Unsteady state experimentation

Unsteady state experiments were carried out in parallel manner on the different Ni and Pt catalysts. Results (Fig. 8) are only shown for Pt-CePr-H and Ni-CePr-H samples which are representative of the diversity on the catalytic results. For Pt-CePr-H, the production of H_2 is low accompanied with a high CO release at 400 °C. At higher temperature, we can observe a sharp hydrogen production in the first seconds with an exponential type decay which stabilizes after 2 min on stream. The initial H_2 production is likely due to methane cracking in the first minute (reaction (6)). Then, the H_2/CO ratio stabilises to 1 which is characteristic of a dry methane reforming type mechanism (reaction (4)). This is corroborated by the shift in time between CO and CO_2 productions and in line with

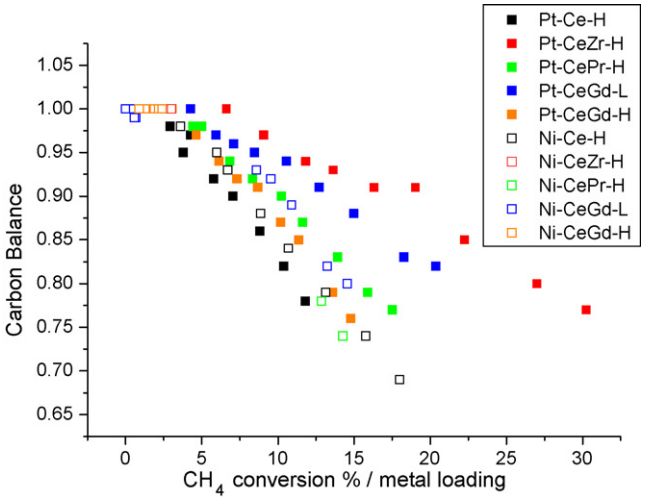

Fig. 7. Carbon balance as a function of the ratio (CH_4 conversion %:% metal loading) and temperature over Pt and Ni-based catalysts under the reacting flow: CH_4:O_2:H_2O:CO_2 = 15:2:20:5 with Ar as balance, flow rate: 50 mL/min.

previous results by Damyanova et al. [11] where Pt-based catalyst is effective for methane dry reforming. Carbon dioxide is first produced by methane deep oxidation in the outset of the catalytic bed and is then converted by dry reforming giving syngas further in the catalytic bed. Similar trends are observed for the Ni catalysts with a much lower CO production and a more rapid decay to reach the steady state. This difference is observable between all Pt and Ni-based catalysts. Over Ni-CePr-H sample and for temperature higher than 450 °C, the H_2/CO ratio is closed to 3 typical of the steam reforming (reaction (3)) reaction. It confirms previous observations where nickel ceria-based catalysts promote methane steam reforming [12]. The profiles of H_2, CO and CO_2 responses are related to the amount of active oxygen which is available for the reaction. In the first second of operations, all oxygen present at the surface may participate to the reaction. Then, the oxygen of the bulk have to migrate to the surface inducing induces a lower kinetic.

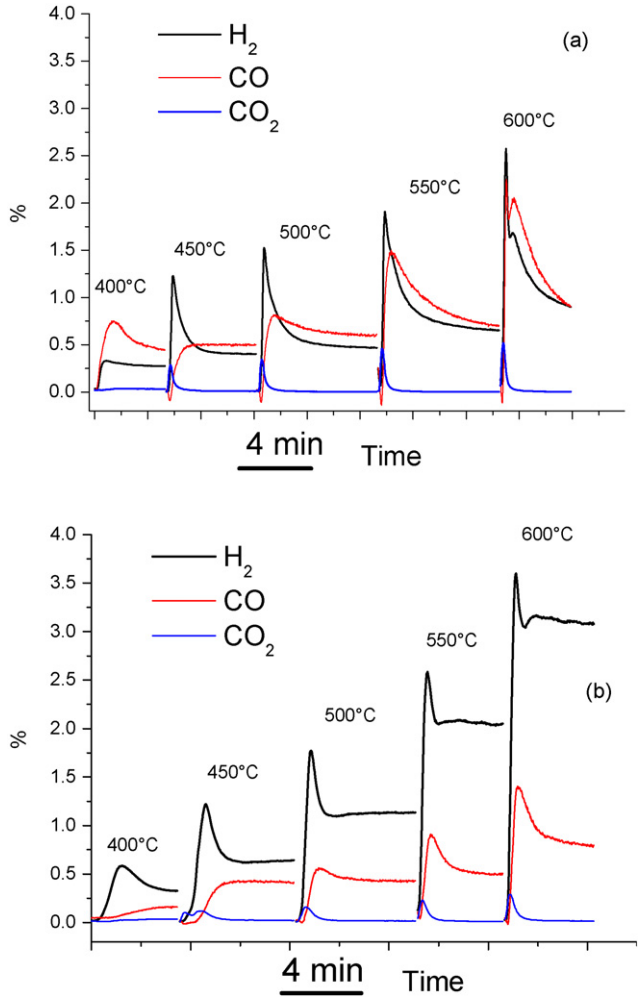

Fig. 8. Transient analyses over Pt-CePr-H (a) and Ni-CePr-H (b) vs. time.

4. Discussion

Reforming including autothermal, dry reforming and partial oxidation on ceria-based catalysts have been widely studied for high temperature conditions [11–15]. Particularly zirconium dopant, known to enhance thermal stability [13], oxygen storage capacity [13] and sintering resistance [14]. We have shown in this study a new picture at low temperature in presence of water and carbon dioxide.

Obviously, the nature of the metal is the most important parameter. Copper-based catalysts lead to combustion without production of H_2 and CO [15,16] whatever the conditions. In contrast, in rich methane condition (Scenario A) Ni and Pt-based catalysts allow the production of syngas. For Ni-based catalysts, the production of H_2, mainly by cracking (reaction 6), is accompanied with a low carbon balance which is mainly due to the formation of carbonaceous species generally in the form of fibers [17]. In addition, the partial reforming of this adsorbed species is support depending. The sample Ni-CeZr-H possesses the upper carbon balance values, while Ni-CePr-H presents the lower, below Ce-H. This disparity could be attributed to a segregation of Pr at the surface of the support due to a redistribution of this cation during the elaboration step [18] as evidenced by Sadykov et al. [19]. This observation associated to the ability to find the Pr cation partly in the +4 state could explain the decrease of surface oxygen vacancies. This accumulation of carbon species is less pronounced over Pt-based catalysts due to the subsequent partial oxidation to CHOx hydrogen carbonate species. Mechanism reaction of methane cracking over Pt-ceria-based catalyst has been pointed out previously in our lab [20] and clearly shows that the oxygen of the support enables to oxidize C deposit over metal via reverse spillover and then that formate ($HCOO^-$) and carbonate (CO_3^{2-}) species are preferentially accumulated at the surface.

Effect of water. The twofold of hydrogen production over Pt-based catalysts compared with tests with Scenario A could be explained as follow: the carbon deposit over the Pt particles is oxidized by bulk oxygen coming from the support. This quantity of oxygen is improved by the dissociation of water into hydroxyl species over support ($2O^* + H_2O = 2OH^*$). Then, CO reacts with these hydroxyl species to produce formate species [20]. Considering the study of Odier et al., no hydroxyl is formed over Pt particles. The higher the oxygen mobility of ceria, the faster C deposit is oxidized. This is shown by the upper and lower values of carbon balance for CeZr-H and Ce-H, respectively, in agreement with their oxygen mobility [21]. An addition of steam over Ni-based catalysts leads to an inhibition at low temperature. The reduction of NiO into Ni did not take place in presence of water. This is likely due to the competitive adsorption of water and methane [10] over Ni and/or NiO particles forming NiOOH species blocking the active sites to methane. The further increase of conversion with temperature is associated to the successive reduction of the nickel particles followed by the methane cracking. The methane steam reform-

ing (reaction (3)) with the dissociative adsorption of water over the support [22] according to: $2H_2O^* \rightarrow 2OH^* + H_2$ with H_2O^* an adsorbed water molecule, explains the improvement at higher temperature. This reaction produces both hydrogen and mobile oxygen species over the ceria support that can oxidize C deposits [23]. Elsewhere, the shift of these OH^* species to the poisoned metal is enhanced by a high oxygen mobility of the support, correlating the upper values of carbon balance obtained notably with CeZr-H support.

Effect of CO_2. The combined effect of water and carbon dioxide over methane oxidation is not common in the literature and constitutes interesting notably for SOFCs systems. The adsorption of carbon dioxide over the cation of the support is effective and form monodentate and bidentate carbonate species as pointed out in our lab by Thinon et al. [22]. These species are able, as a function of support oxygen mobility, to move towards the metal and to oxidize CHx deposits. This main involvement of oxygen mobility is suggested in Fig. 7 where the Pt-based catalyst with the highest dopant loading presents the upper carbon balance values contrary to Ce-H with limited oxygen mobility. We have demonstrated a high dependence of support for methane conversion over Ni-based catalysts when CO_2 is added to the stream. The catalysts presenting previously the better results associated to their high oxygen mobility (Ni-CeZr-H and Ni-CePr-H) are here fully non-selective for syngas generation. Here again, the suggested additional adsorption of CO_2 over the support and its motion to the metal is too important to keep metallic active nickel particles.

5. Conclusion

The HT approach has enabled to assess catalytic properties of various catalysts with different metal, support and porous structures. In contrast to classical anode catalysts for high temperate SOFC, Ni-based catalysts are not appropriate since Ni can be partially oxidized at low temperature (500–600 °C). On the other hand, Pt cerium-based catalysts are interesting candidates as anode components. More specifically, Pt-based catalysts with high oxygen mobility such as Pt-CeZr-H are the best candidates in presence of water and carbon dioxide as found in SOFC (high methane conversion and H_2 yields combined with high carbon balance). The combinatorial approach, combined with parallel transient investigations, has enabled to suggest possible mechanism of activation/inhibition of catalysts.

Acknowledgements

Authors thanks ADEME (Agence de l'Environnement de la Maîtrise de l'Energie) and Région de Bourgogne for the financial support. Scientific services of IRCELyon are fully acknowledged. Rhodia is also acknowledged for providing ceria supports.

References

[1] H. Timmermann, D. Fouquet, A. Weber, E. Ivers-Tiffée, U. Hennings, R. Reimert, Fuel Cells 6 (3–4) (2006) 307–313.
[2] R.J. Gorte, et al., Solid State Ionics 175 (1–4) (2004) 1–6.
[3] J. Beckers, et al., Green Chemistry 11 (7) (2009) 921–925.
[4] Y. Shiratori, et al., Journal of Power Sources 180 (2) (2008) 738–741.
[5] F. Chen, et al., Solid State Ionics 166 (3–4) (2004) 269–273.
[6] G. Morra, et al., Chemical Engineering Journal 138 (1–3) (2008) 379–388.
[7] W. Cai, et al., Catalysis Today 138 (3–4) (2008) 152–156.
[8] J.R. González-Velasco, et al., Applied Catalysis B: Environmental 12 (1) (1997) 61–79.
[9] H.-S. Roh, et al., Catalysis Letters 74 (1) (2001) 31–36.
[10] N. Laosiripojana, et al., Chemical Engineering Journal 138 (1–3) (2008) 264–273.
[11] S. Damyanova, et al., Applied Catalysis B: Environmental 89 (1–2) (2009) 149–159.
[12] T.-J. Huang, et al., Applied Catalysis A: General 302 (2) (2006) 325–332.
[13] A. Trovarelli, et al., Chemtech 27 (6) (1997) 32–37.
[14] B.C.H. Steele, Solid State Ionics 129 (1–4) (2000) 95–110.
[15] H. Kim, et al., Journal of the Electrochemical Society 149 (3) (2002) A247–A250.
[16] A. Sin, et al., Journal of Power Sources 164 (1) (2007) 300–305.
[17] T. Takeguchi, et al., Journal of Power Sources 112 (2) (2002) 588–595.
[18] M.P. Rodriguez-Luque, et al., The Journal of Physical Chemistry C 112 (15) (2008) 5900–5910.
[19] V.A. Sadykov, et al., Reaction Kinetics and Catalysis Letters 86 (1) (2005) 21–28.
[20] E. Odier, et al., Catalysis Today 127 (1–4) (2007) 230–237.
[21] M. Salazar, et al., Applied Catalysis A: General 310 (2006) 54–60.
[22] O. Thinon, et al., Topics in Catalysis 52 (13) (2009) 1940–1945.
[23] T.-J. Huang, et al., Catalysis Letters 105 (3) (2005) 239–247.